AGU ADVANCING EARTH AND SPACE SCIENCES

JGR Oceans

RESEARCH ARTICLE
10.1029/2025JC022716

Ocean Constraints on Winter Antarctic Sea Ice Extent

W. R. Hobbs[1], Ryan Holmes[2], and Andrew E. Kiss[3]

[1]Australian Antarctic Program Partnership, Institute for Marine and Antarctic Studies, University of Tasmania, Hobart, TAS, Australia, [2]Australian Bureau of Meteorology, Sydney, NSW, Australia, [3]Research School of Earth Sciences, Australian National University, Canberra, ACT, Australia

Key Points:

- The winter Antarctic sea ice extent maximum is constrained by the ocean's capacity to maintain a surface freezing temperature
- A metric–Stability at Freezing Temperature–is introduced to quantify the ocean cooling that must occur before sea ice can freeze
- This framework identifies the northern limit of Antarctic sea ice, and offers a tool to understand recent extreme winter sea ice extents

Supporting Information:

Supporting Information may be found in the online version of this article.

Correspondence to:

W. R. Hobbs,
will.hobbs@utas.edu.au

Citation:

Hobbs, W. R., Holmes, R., & Kiss, A. E. (2026). Ocean constraints on winter Antarctic sea ice extent. *Journal of Geophysical Research: Oceans*, *131*, e2025JC022716. https://doi.org/10.1029/2025JC022716

Received 3 APR 2025
Accepted 6 JAN 2026

Author Contributions:

Conceptualization: W. R. Hobbs
Data curation: Ryan Holmes
Formal analysis: W. R. Hobbs, Ryan Holmes, Andrew E. Kiss
Methodology: W. R. Hobbs, Ryan Holmes, Andrew E. Kiss
Resources: Ryan Holmes
Visualization: W. R. Hobbs
Writing – original draft: W. R. Hobbs
Writing – review & editing: Ryan Holmes, Andrew E. Kiss

Abstract Winter Antarctic sea ice extent has historically shown relatively low variability compared to warmer seasons, but recent winters have shown very extreme low ice cover. As a result, there is significant interest in understanding the physical constraints on winter Antarctic sea ice cover. In this work the ocean's role in constraining maximum extent is explored. Using basic physical principles, the concept of “Stability at Freezing Temperature” is introduced, and then applied to calculate the total ocean heat that must be lost to the atmosphere before sea ice can begin to form. This method is found to capture spatial and interannual variability of the winter sea ice edge, including during recent extreme sea ice cover states. This framework can be used to separate the effects of ocean thermal and haline anomalies on the ice edge. It is also used to quantify the contributions from summer preconditioning, atmospheric cooling, and subsurface ocean heat transport, all of which are shown to contribute significantly to winter ice extent variability. This method provides an invaluable tool for understanding recent sudden changes in Antarctic sea ice cover.

Plain Language Summary Recent Antarctic winters have seen unusually low sea ice cover, sparking interest in what controls this. This study looks at how the ocean affects the maximum extent of winter sea ice. It introduces the idea of “Stability at Freezing Temperature,” which is a physically-based metric that can be used to quantify how much heat must be lost from the ocean to the atmosphere before sea ice can form. This approach helps show how past summer conditions, winter cooling, and upward mixing of ocean heat each influence how far sea ice spreads in winter. This method has clear relevance to understanding recent extremely low winter sea ice conditions.

1. Introduction

Every year Antarctic sea ice grows from a summer minimum of approximately 2 million km^2 to a winter maximum of 17 million km^2. However, even though the mean winter extent is more than 8 times that of summer, the winter standard deviation is approximately the same as summer, and much less than the equinoctial seasons (Figure 1a). There have been multiple extreme low sea ice summers (Eayrs et al., 2021; Liu et al., 2023; Raphael & Handcock, 2022; Turner et al., 2017), but until very recently winter extreme events of a similar relative magnitude had never been observed. Moreover, Antarctic sea ice trends from 1979 to 2015 had a distinct seasonality, with trends being more intense and statistically-significant in warmer seasons compared to winter (Hobbs et al., 2016). The seasonality of both the trends and the interannual variability suggest that there exists some constraint on maximum Antarctic sea ice extent which restricts its ability to fluctuate from year to year. However, recently that constraint seems to have relaxed, with a widely-reported extreme low winter sea ice in 2023 (Purich & Doddridge, 2023), which was repeated in 2024 and to a lesser degree 2025. The magnitude of the 2023 event - more than 5 standard deviations below the 1979–2018 climatology (Gilbert & Holmes, 2024) - and the winter timing motivate an examination of constraints on winter sea ice.

Sea ice is formed by the atmosphere removing heat from the ocean, but there is significant surface cooling in the Southern Ocean north of where the maximum ice edge occurs (Figure 1b). This implies that atmospheric cooling is not the sole constraint on how far north the ice can grow, and the ocean also plays a role. The existence of an ocean constraint on sea ice is consistent with the climatological mean and variance pattern in Figure 1a. Autumn growth (March–June) has a very rapid northward expansion of the ice edge (indicated in Figure 1a by rapidly increasing SIE), but eventually in mid-winter (July–August) the sea ice hits some limiting factor despite continuing cold atmospheric conditions. This limiting factor both slows the growth rate and limits year-to-year variability of the maximum extent.

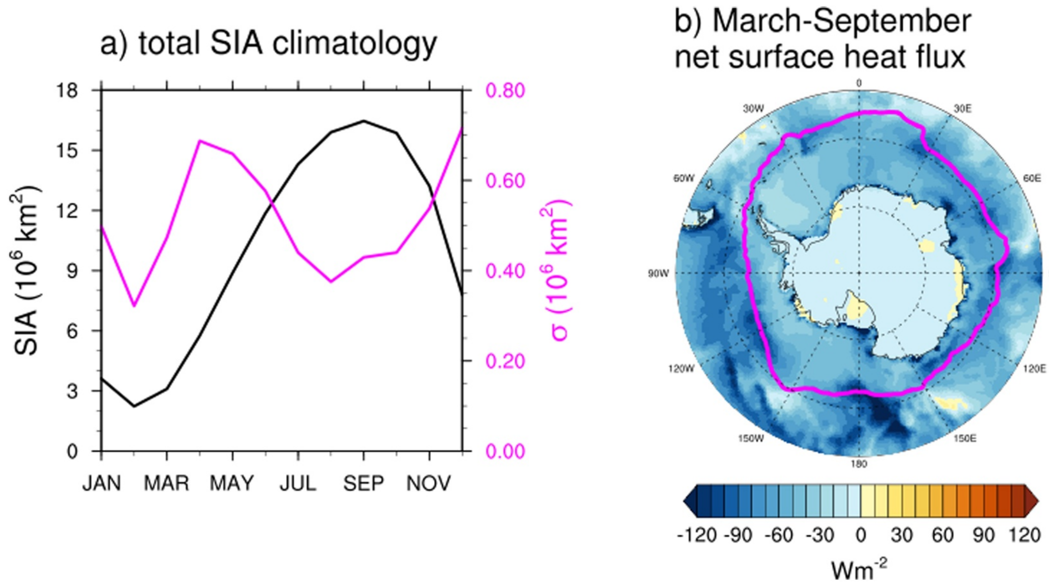

Figure 1. (a) 1980–2021 Antarctic sea ice area climatological mean (black line; left *y*-axis) and standard deviation, σ (magenta line; right *y*-axis). (b) 1980–2021 March-September mean net surface heat flux (Wm^{-2}) from ERA5 reanalysis (positive indicates heat into ocean/sea ice). Magenta line shows the September mean ice edge (i.e., 15% sea ice concentration isoline) from NSIDC climate data record satellite sea ice concentration observations.

The polar Southern Ocean is characterized as a "β-regime" water column, which is to say that seawater buoyancy (and therefore stratification) is dominated by haline rather than thermal conditions (e.g., Roquet et al., 2022). This means that the upper ocean can maintain a temperature inversion, with cold but relatively fresh water on top of warm, saltier water. Sea ice itself is the dominant surface freshwater forcing (Abernathey et al., 2016; Pellichero et al., 2017), since brine rejection from sea ice freezing makes the mixed layer saltier and denser. With sufficient sea ice growth, the surface water becomes dense enough to sink and entrain warm deep water into the mixed layer, causing a vertical heat flux that melts some of the newly-formed sea ice. This balance between production and melt has been shown to place a constraint on net winter sea ice growth (Martinson & Iannuzzi, 1998; Wilson et al., 2019), with the strength of the constraint being a function of how much salt input is required to entrain deep water. However, since this mechanism is driven by sea ice-related brine rejection, it implicitly presupposes that sea ice can initially form. As such, it is an important limit on sea ice thickness, but not necessarily a limit on where sea ice can exist in thermal equilibrium with the ocean (noting that sea ice can exist out of equilibrium briefly when associated with sea ice transport, e.g. Su (2017)).

Using an ocean state estimate (i.e., a model solution constrained by observations), Su (2017) demonstrated a remarkably close correspondence between the climatological winter maximum ice edge and the northern limit of the β-regime (i.e., where the upper ocean transitions from haline-dominated to thermally-dominated stratification). This correspondence is imperfect, due to the effect of mesoscale eddies and sea ice dynamics at the ice edge (Su, 2017). Whilst robust, this climatological perspective does not allow a consideration of other factors that might affect year-to-year differences in the winter ice edge, for example, heat anomalies from the preceding summer (Himmich et al., 2024) or surface cooling over winter (J. Wang et al., 2024).

Given recent extreme low winter freeze seasons, there is clear need for a physical framework that can quantify the limits on winter sea ice cover, and how those limits may be changing. In this work a metric called Stability at Freezing Temperature (SaFT) is introduced, with the aim of developing a diagnostic framework that can disentangle the effects of ocean thermal and haline anomalies on sea ice in this tightly coupled system. This metric is shown to have strong agreement with winter ice extent in both reanalysis and an ocean-sea ice model, and can be applied to separate the thermal, haline and surface flux conditions that set the winter sea ice maximum.

2. Data

2.1. Observations

The subsurface temperature and salinity structure is characterized using the European Centre for Medium-Range Weather Forecasts ORAS5, a global ocean reanalysis of quality controlled ocean observations, combined with the NEMO ocean model (Zuo et al., 2019). ORAS5 has a ¼^{o} horizontal resolution, with 1–20 m vertical resolution (increasing with depth) in the upper 200 m that is most relevant for this study. The polar Southern Ocean is critically under-observed especially in the austral winter, which has been a considerable impediment to research (SOOS, 2023). The observational part of this study is restricted to post-2006, when the advent of the polar Argo program made analysis of circumpolar variability somewhat feasible (Figure S1 in Supporting Information S1). The Antarctic continental shelf still has very few observations, challenging studies of summer sea ice which is largely restricted to the near-coastal environment. The winter ice edge is in the open ocean and is much better observed.

Sea ice cover is represented using version 4 of the monthly-mean National Snow and Ice Date Center Climate Data Record (CDR) of sea ice concentration (Meier et al., 2021). A sea ice concentration of 15% is used to represent the northern edge of the winter ice pack.

We use net surface heat fluxes (e.g., Figure 1) estimated from version 5 of the European Centre for Medium-range Weather Forecasts Reanalysis (ERA5; Hersbach et al., 2020). The net surface heat flux is calculated as the sum of the net shortwave, net longwave, and sensible and latent heat fluxes, where a negative sign implies ocean cooling. ERA5 has a proven high-quality representation of the atmosphere over the polar Southern Ocean, although like many reanalyzes and model products there is a cloud-related downwelling longwave radiation negative bias (H. Wang et al., 2020), implying an overestimate of the net surface ocean cooling. Due to very few direct observations of turbulent heat fluxes (i.e., sensible and latent heat) the exact numerical bias on the net surface flux is very difficult to ascertain.

2.2. ACCESS-OM2 Ocean-Sea Ice Model

Due to the temporal limits of sub-surface ocean data and the uneven spatial coverage, the same analysis is performed using the ¼^{o} resolution ACCESS-OM2-025 ocean-sea ice model. The model formulation is described in detail in Kiss et al. (2020), but briefly the ocean component is the Geophysical Fluid Dynamics Laboratory Modular Ocean Model v5.1 (MOM5), and the sea ice model is the Los Alamos sea ice model version 5.1.2 (CICE5). The ¼^{o} model used here has 50 vertical levels in total, with 18 of these levels within the upper 200 m, and a 2.3 m vertical resolution at the surface.

Typically the model is run using atmospheric boundary conditions from the JRA55-do reanalysis (Kiss et al., 2020). The experiment analyzed here has instead been forced with the ERA5 reanalysis from 1980 to 2021; this allows a direct comparison with the observation-based analysis which also uses ERA5 and gives a slight improvement in the representation of Antarctic sea ice. Note however that the model's latent and sensible air-sea heat fluxes are computed via bulk formulae that depend on the model sea surface temperature, as does the upward longwave radiation, and thus these components will differ from the air-sea fluxes taken directly from the ERA5 reanalysis. The model has some bias in total sea ice area (SIA), but monthly anomalies are strongly constrained by the atmospheric forcing and the model represents month-to-month variability remarkably well (Figure S2 in Supporting Information S1).

3. Method

For a sea ice floe to exist for anything but the most transient timescale (hours to days) it must be in thermal equilibrium with the underlying ocean, so a precondition for sea ice to start forming is that the ocean surface must be cooled to the local freezing temperature, T_f. As the surface water cools it becomes denser, it sinks and is replaced at the surface by warmer water which then also must be cooled. Considering the effect of cooling alone (i.e., neglecting turbulent mixing, freshwater fluxes and horizontal advection), the depth to which it will sink is set by the vertical salinity gradient, $\frac{\partial S}{\partial z}$; if the deeper water is sufficiently salty compared to the surface water, it can maintain a stable stratification even though the shallower water is colder (Figure 2). From this premise the concept of SaFT can be introduced, which is simply a measure of whether a surface parcel of water will sink or remain at

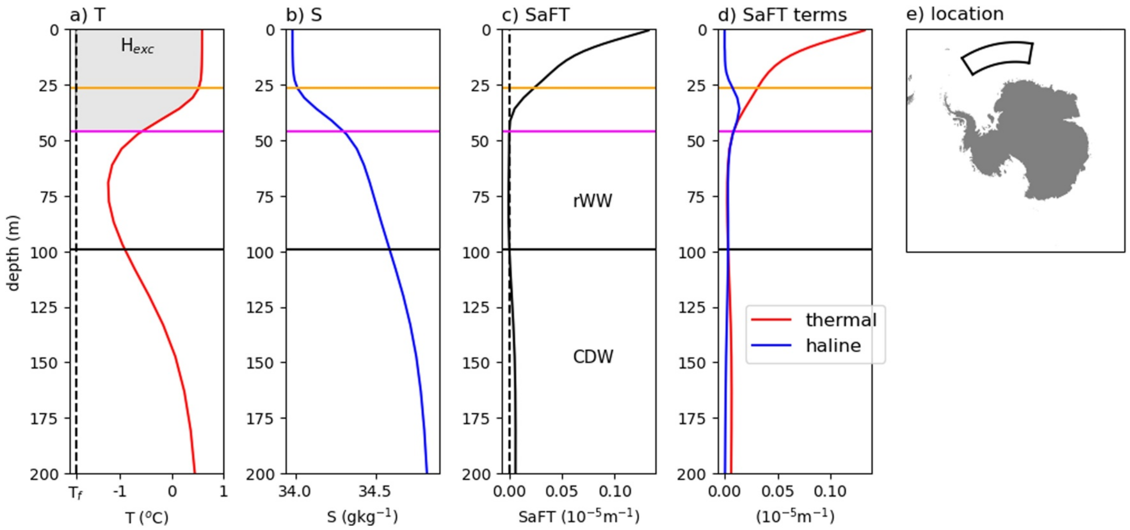

Figure 2. 2006–2023 ORAS5 February climatology of (a) Temperature (b) Absolute Salinity, (c) Stability at Freezing Temperature (SaFT) and (d) decomposition of SaFT into a salinity term (blue line $= \beta \frac{\partial S}{\partial z}$) and a temperature term (red line, $\alpha \frac{T - T_f}{\Delta z}$), as per Equation 1. Data is averaged over the region of the Weddell Sea (33°W–10°E, 69°–65°S) shown in panel (e). The magenta and black lines show the upper and lower (respectively) limits where SaFT = 0, and the orange horizontal line shows the mixed layer depth. The gray polygon in (a) indicates the excess heat above freezing (H_{exc}) in Equation 2.

the surface when cooled to T_f. For data that is in discrete vertical coordinates (which is the case for almost all observations and model output), this can be expressed as:

$$\text{SaFT} = \alpha \frac{(T - T_f)}{\Delta z} - \beta \frac{\partial S}{\partial z} \tag{1}$$

where α is the thermal expansion coefficient, β is the haline contraction coefficient, and Δz is the vertical resolution of the data. α and β are calculated here using the TEOS 10 Equation of State. When SaFT > 0, the parcel's potential density at the freezing temperature is greater than the water below and it must sink; when SaFT < 0 the parcel will remain buoyant even at the freezing temperature. The vertical salinity gradient is estimated here using a centered finite difference.

Whilst the salinity term in Equation 1 is a gradient that adjusts to the actual vertical resolution, the temperature term is a difference with the approximately-constant T_f (rather than with temperature at an adjacent level). Therefore, the temperature term is dependent on the vertical resolution of the data Δz. Our tests indicate that the calculation is relatively insensitive to vertical resolution as long as the warm, fresh summer surface layer is resolved, but at resolutions coarser than 15 m this layer is not resolved (see Figure S3 in Supporting Information S1).

Sinking water will be replaced at the surface by another parcel which must then also be cooled. Therefore the entire layer of sea water between the surface and the shallowest SaFT = 0 isoline must be cooled before a surface freezing temperature (T_f) can be stably maintained, assuming no vertical heat flux from mixing. This means that the minimum amount of heat that must be removed before freezing can occur (i.e., the "excess" heat), H_{exc}, can be estimated as:

$$H_{\text{exc}} = \int_{z(\text{SaFT}=0)}^{z=0} \rho c_p \left(T(z) - T_f\right) dz \tag{2}$$

where ρ, c_p are the seawater density and specific heat capacity, respectively. $H_{\text{exc}} \leq 0$ is therefore a necessary precondition for sea ice formation. Furthermore, since H_{exc} integrates information about the thermal and stratification state of the ocean, it can be used to explore the conditions that constrain winter sea ice.

(Note that for plotting purposes, given noise in the observational data and the fact that $H_{exc} = 0$ is the theoretical minimum value, the zero isoline is difficult to map coherently and thus a small positive value is more appropriate. In Figures 3, 4 and 6 a value of $H_{exc} = 0.05$ GJm^{-2} is used. This is equivalent to the heat required to melt 16.5 cm of sea ice, assuming a sea ice density of 905 kgm^{-3} and latent heat of freezing of 334 kJkg^{-1}. For context 20 cm is the minimum observable thickness from passive microwave satellite retrievals e.g. Nihashi and Ohshima (2015)).

This construction is demonstrated in Figure 2 for a February areal-mean profile. Since the sea ice growth season starts in late February, this represents end-of-summer preconditioning. The condition SaFT = 0 separates the upper ocean water column into 3 layers (Figure 2c). From the surface to the shallowest SaFT = 0 isoline (magenta line) is a warm, fresh layer that has developed over summer from sea ice melt and solar heating. This is the layer that must be initially cooled (i.e., H_{exc} removed) before ice can form at the surface, indicated by the gray polygon in Figure 2a.

Below this line is a cold and salinity-stabilized layer of remnant Winter Water (rWW), which is the cold water formed during the previous winter's sea ice growth (this layer is also partially thermally-stratified from 25 to 75 m, Figure 2a). Below the rWW layer the profile returns to a thermally dominated regime (i.e. SaFT > 0) indicating the transition to warm, salty Circumpolar Deep Water (CDW). The CDW and rWW are not initially thermal barriers to sea ice formation but will be returned to later in this paper.

Importantly, Figure 2 demonstrates that the SaFT parameter unambiguously identifies well-established features of the polar ocean vertical profile based on physical first-principles. For comparison, Figure 2 also shows the Mixed Layer Depth (MLD), defined here as the depth at which the potential density is 0.03 kgm^{-3} greater than the surface density (Levitus, 1982). The MLD identifies the almost isothermal and isohaline surface layer, that is well-mixed largely due to mechanical mixing driven by surface turbulence. However, as noted, maintaining a surface temperature of T_f requires a non-zero vertical salinity gradient (which is impossible in an isohaline layer), and so the mechanically-developed mixed layer does not represent the depth to which surface freezing water would sink. Therefore, using MLD instead of SaFT to estimate H_{exc} would underestimate the thermal barrier to freezing.

H_{exc} is a bulk thermodynamic metric that does not account for sea ice processes, in particular sea ice transport, that might also influence the ice edge; the implications of this caveat are explored formally in the next section.

4. Results

4.1. Climatological Limits to Ice Growth

The evolution of H_{exc} over the sea ice growth season (Figure 3) demonstrates a close correspondence between the sea ice extent (cyan line) and the limit $H_{exc} \sim 0$ (magenta line). The ice edge and the H_{exc} isolines are approximately collocated in all months, indicating that H_{exc} exerts a control on the ice extent in both the model and reanalysis, demonstrating the strong relationship between H_{exc} and the ice edge.

However the ice edge is often north of the $H_{exc} \sim 0$ isoline in Figure 3. This is because H_{exc} is a bulk thermodynamic metric that does not account for sea ice transport, and in late winter the ice edge creeps north of the $H_{exc} = 0.05$ GJm^{-2} limit due to northward sea ice drift (Su, 2017). Analysis of the thermodynamic freezing/melting rate of sea ice in the model (Figure 4) demonstrates that sea ice melts north of the H_{exc} limit, and sea ice there can only be maintained by constant advective replenishment from further south (Himmich et al., 2023). This confirms that $H_{exc} \sim 0$ is a strict thermodynamic limit on sea ice formation, but not necessarily on advected sea ice cover.

Figure 3 shows extensive ocean regions that are not shaded at all. In thermally-dominated stratification regions where SaFT is never negative, conceptually a surface parcel cooled to the freezing temperature should sink to the sea floor (although in practice it will mix with ambient waters during descent), so that the "true" value of H_{exc} can be approximated as the integral of heat content relative to the freezing temperature of the entire water column. For convenience, and to visually emphasize the importance of the SaFT control, such regions are masked (white) in Figure 3, and so only regions where halo-stratification occurs (i.e., where SaFT ≤ 0 at some depth) are shaded. The sea ice pack occurs only within these shaded regions, demonstrating that halo-stratification is a necessary condition for sea ice. Indeed, it seems to be the dominant constraint in the reanalysis and does not change much over the course of winter (even though H_{exc} does). However, the main difference between the model and the

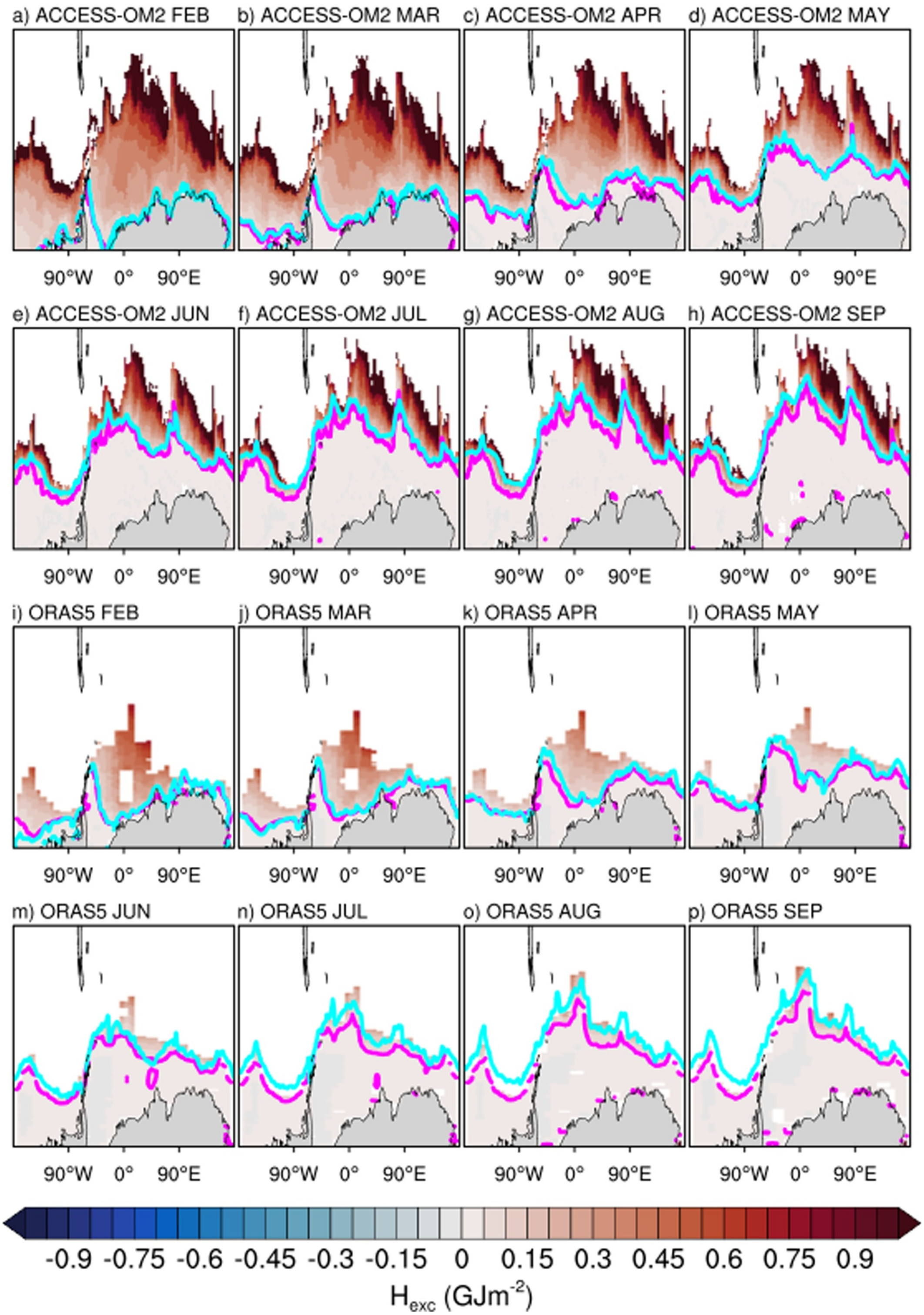

Figure 3. Monthly climatological excess heat above freezing, $H_{exc,}$ integrated from the surface to the Stability at Freezing Temperature (SaFT) = 0 isoline (GJm^{-2}; Equation 2 and Figure 2a) from (a–h) 1980–2021 ACCESS-OM2 and (i–p) 2006–2023 ORAS5. The cyan lines show the mean ice edge (SIC = 15%), and the magenta lines show the H_{exc} = 0.05 GJm^{-2} contour. Regions where the water column is not sufficiently halo-stratified to allow negative SaFT values are unshaded.

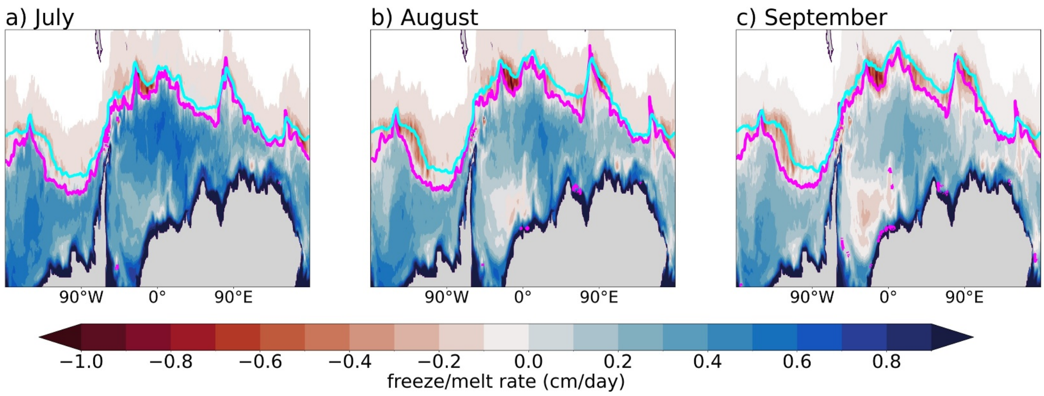

Figure 4. 1980–2021 climatological mean ACCESS-OM2 thermodynamic sea ice freeze/melt (cm/day). The magenta line shows the $H_{\mathrm{exc}} = 0.05$ GJm^{-2} isoline, and the cyan line shows the sea ice edge (i.e., SIC = 15% isoline). Note that where the ice edge is north of the thermodynamic limit set by $H_{\mathrm{exc}} = 0.05$ GJm^{-2}, this is exclusively in regions of net sea ice melt (red shading).

reanalysis is that the model supports halo-stratification much further north. This implies a fresh Southern Ocean surface bias in the model, which is beyond the scope of this work to investigate. The key result is that, despite the deficiencies in both the model and observing network, both show a very similar qualitative relationship between the ice edge and the $H_{\mathrm{exc}} \sim 0$ limit.

Figure 3 demonstrates the constraint that H_{exc} places on ice growth, so it is useful to consider how it responds as the water column changes over winter. Figure 5 shows the winter evolution of temperature, salinity and SaFT for the same Weddell Sea domain as Figure 2. The layer definitions are exactly as for Figure 2, with magenta and black lines showing the shallowest and deepest SaFT = 0 isolines respectively, separating (in order of increasing

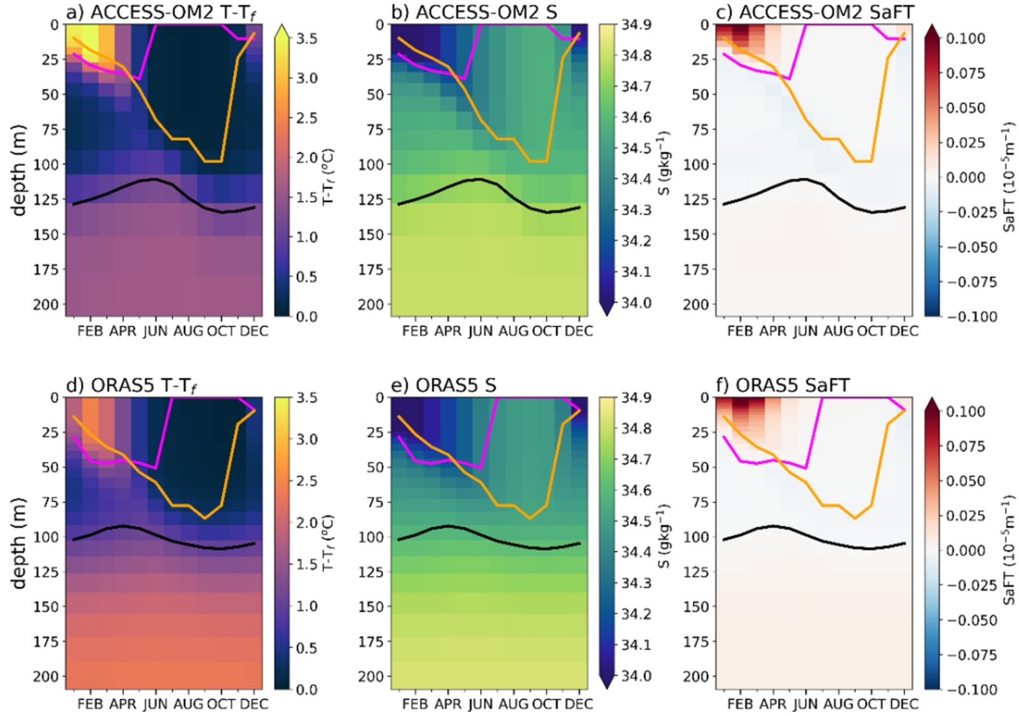

Figure 5. Monthly climatological profiles of T-T$_f$ (left column), S (middle), and Stability at Freezing Temperature (SaFT) (right), for the Weddell sector (as per Figure 2) for (a–c) 1980–2021 ACCESS-OM2 and (d–f) 2006–2023 ORAS5 data. As for Figure 2, the magenta and black lines show the upper and lower SaFT = 0 isolines, and the orange line shows the mixed layer depth.

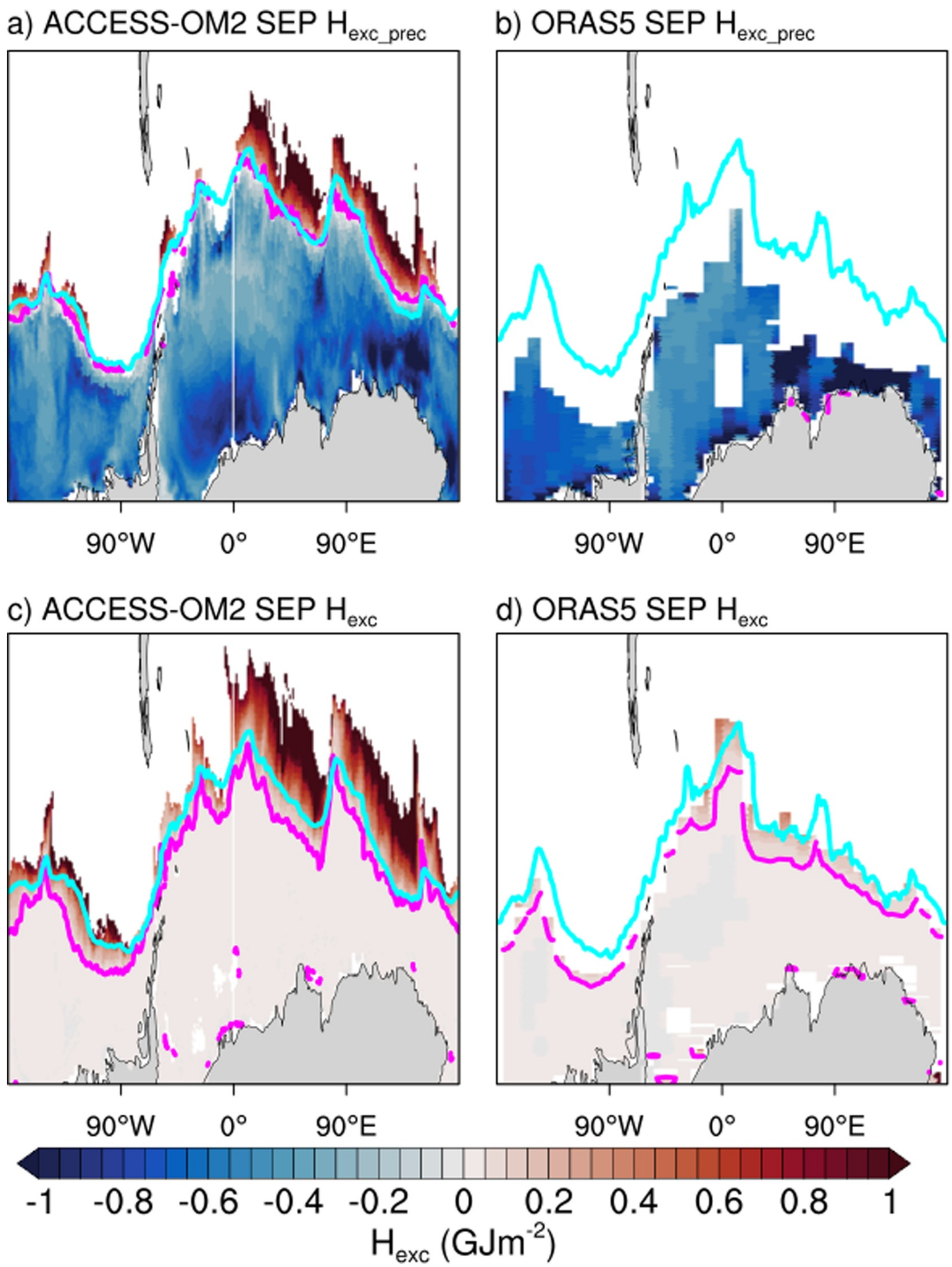

Figure 6. September H_{exc_prec} estimated from the sum of H_{exc} in February and March-September time-integrated surface cooling (Q_{sfc}), for (a) 1980–2021 ACCESS-OM2 and (b) 2006–2023 ORAS5. The cyan line shows the September mean ice edge and the magenta line shows the $H_{\mathrm{exc}} = 0.05$ GJm^{-2} isoline. Panels (c) and (d) show the directly calculated September H_{exc} (i.e., replications of Figures 3h and 3p respectively).

depth) the summer surface layer from the rWW, and the rWW from CDW. Initially, the fresh and warm summer layer which contains the H_{exc} (Figure 2a) must be cooled before sea ice can grow. As in Figure 2, the MLD (orange line in Figure 5) is shallower in the summer and autumn than the layer defining H_{exc}. As the surface cools, buoyancy is lost, causing the surface layer to deepen and mix with the higher salinity rWW from below.

Journal of Geophysical Research: Oceans 10.1029/2025JC022716

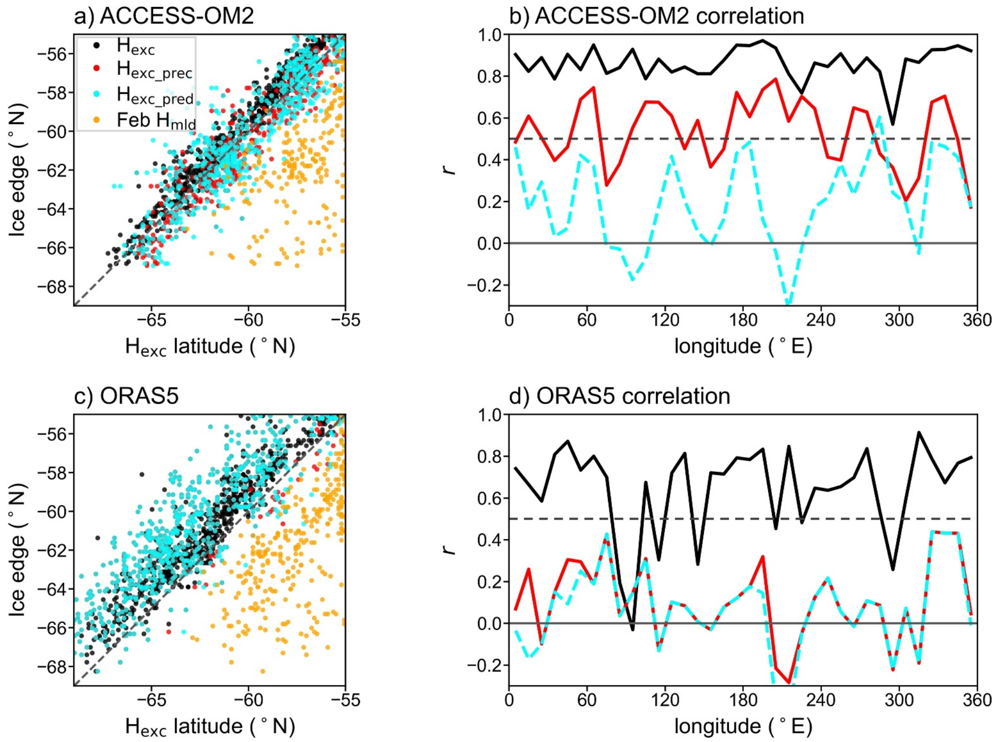

Figure 7. Relationship between the September ice edge latitude and the latitude of the September $H_{\text{exc}} = 0.05\ \text{GJm}^{-2}$ isoline over the 2006–2021 period. Panels a and c show scatter plots of the latitudes of the September sea ice edge (y axes) and the September $H_{\text{exc}} = 0.05\ \text{GJm}^{-2}$ isoline for each year, estimated using September ocean conditions (black dots); and $H_{\text{exc\_}prec}$ (February ocean conditions combined with interannually-varying winter coolin; red dots; viz Figure 6) and $H_{\text{exc\_}pred}$ (February ocean conditions combined with climatological-mean winter cooling; cyan dots). Orange dots show an estimate using the February mixed layer depth (MLD) and interannually-varying winter cooling, as a direct comparison to $H_{\text{exc\_}prec}$. Panels b and d show the interannual correlation by longitude with the same color scheme (MLD is not shown), where the dashed horizontal lines indicate a 95% statistically-significant correlation.

Eventually the complete removal of H_{exc} is achieved by June, in both the model and ORAS5. The temperature of the surface layer is approximately T_f (i.e., $H_{\text{exc}} = 0$; Figures 5a and 5d), and the near surface SaFT is close to zero indicating a salinity-stabilized regime (Figures 5c and 5f). At this point the system has transitioned to a winter regime as described by Martinson (1990), whereby sea ice growth has begun and sensible cooling of the near surface water is replaced by brine rejection due to sea ice growth, salinifying the surface layer (Figures 5b and 5e). Since the summer H_{exc} shown in Figure 2a has now effectively been completely destroyed, the upper SaFT = 0 line (i.e., the magenta line) is meaningless, and we set it to the surface. It re-emerges again in December, as spring melt and surface warming cause the development of the summer surface layer.

Whilst the focus of this work is on what limits initial sea ice formation, it is useful to consider whether the SaFT metric provides useful information in the winter regime dominated by brine rejection. The MLD accurately identifies the approximately isohaline surface layer at freezing temperature, but the SaFT metric provides further information. The black line (i.e., the deeper SaFT = 0 isoline in Figure 5) shows the CDW/WW boundary which deepens once the winter regime is reached in June. This is because brine rejection from sea ice growth entrains warm deep water. However, the layer of negative (blue) SaFT between the freezing WW and the deep water shows that the entrainment rate is limited by the salinity gradient. The heat in in this layer has been termed the "Thermal Barrier," since it prevents complete destabilization of the water column, either by preventing further sea ice growth (and thus brine rejection), or by melting some ice and freshening the surface layer (Martinson, 1990; Martinson & Iannuzzi, 1998). Thus, the Thermal Barrier limits sea ice but also maintains the vertical salinity gradient. If there were no SaFT layer, the system would be thermally destratified, resulting in the loss of all sea ice and deep open water convection, as is observed periodically in the Weddell polynya (Martinson, 1990). These concepts have been well-addressed by previous work (Martinson, 1990; Martinson & Iannuzzi, 1998; Wilson et al., 2019), but SaFT quantifies the depth and stratification of the "Thermal Barrier" layer in a single simple metric.

From the winter evolution shown in Figure 5, a simplified formulation suggests that the winter sea ice extent is the product of three factors:

1. *Preconditioning*, that is, the thermal and haline state of the ocean at the end of summer (e.g., Himmich et al., 2024)
2. *Cooling*, that is, ocean-atmosphere heat flux over winter that removes H_{exc}, which is largely a function of meteorological conditions
3. *Ocean heat flux*, that is, movement of heat into the layer above SaFT = 0, either from the deep ocean through vertical mixing, or through lateral advection/eddy heat transport. Only the former is considered here since it is related to sea ice-ocean feedbacks.

The impact of just the first two factors—preconditioning and atmospheric cooling—can be isolated by estimating H_{exc} in February, and then subtracting the climatological surface cooling integrated from the beginning of March (the approximate start of the sea ice growth season) to the month of interest (Figure 6; note that the blue shading in Figures 6a and 6b indicates cooling that has been used for sea ice production or to cool entrained warm deep water). For simplicity we focus here on a single month, September, since this marks the end of the freezing season and so the atmosphere has had the longest possible opportunity to overcome the ocean constraint. Figure 3 indicates that we would see qualitatively similar H_{exc}-ice edge relationships for any winter month.

For the model, the near-zero isoline of this preconditioned estimate of H_{exc} (termed here H_{exc_prec}) is closely related to the winter ice edge (Figure 6a), demonstrating that ice formation is constrained by the combination of ocean conditions at the start of the growth season (preconditioning) and winter cooling. Interestingly, for the model the H_{exc_prec} limit agrees with the September ice edge better than the H_{exc} from the September water column (i.e., Figure 6c, which is a reproduction of Figure 3h). In the latter case the calculation of H_{exc} includes vertically-entrained heat, which explains why H_{exc} in Figure 6c is higher than H_{exc_prec} in Figure 6a. If the primary means of entrainment is brine rejection during freezing, then the extra heat contained in H_{exc} not captured by H_{exc_prec} is a barrier to sea ice thickening once freezing has begun (Martinson & Iannuzzi, 1998), but it is not a limit on the ice edge latitude (but further implying that entrainment is the heat source that melts ice near the ice edge in Figure 4).

The relationship between late winter sea ice and February-derived H_{exc_prec} does not work so well for the reanalysis, with the ice edge occurring north of the limit (Figure 6b). However, this relationship is appreciably better when using September hydrographic data to calculate September H_{exc} (Figure 6d), and unlike the model suggests that summer preconditioning is not a useful indicator of the winter ice edge. Instead, in the reanalysis the latitude at which there is a sufficiently haline-dominated stratification to allow a SaFT layer (recalling that the unshaded regions in Figure 6 show where no SaFT layer is detected) is much more dominant a constraint. This implies that either the February salinity profiles in ORAS5 have too weak a salinity gradient in the winter marginal ice zone, or that the near-surface salinity develops over winter (perhaps through melt of northward transported sea ice), in a way not captured by the ACCESS-OM2 model. We do not explore that question further here, whilst noting that it has implications for studies of winter sea ice predictability.

4.2. Interannual Variability

The role that H_{exc} plays in limiting winter sea extent is very clear in the climatological mean, but does it affect interannual sea ice variability? To explore this, the September-mean ice edge latitude (averaged over 10° longitude bands) is compared with the latitude of the September $H_{\mathrm{exc}} = 0.05\ \mathrm{GJm}^{-2}$ isoline from year to year (black lines and dots in Figure 7). Scatterplots (Figures 7a and 7c) conflate both spatial and interannual variability, whilst correlations (Figures 7b and 7d) focus on interannual variability.

The model shows a remarkably high spatial and temporal correlation between the ice edge and H_{exc} (Figures 7a and 7b), with interannual correlations greater than 0.8 for nearly all longitudes except near the sea-ice-free Antarctic Peninsula (300°E). The relationship is also very strong for ORAS5, albeit weaker than the model (Figures 7c and 7d). The interannual correlation is statistically significant in most longitudes, except off the East Antarctic coast between 70° and 100°E, a region that combines relatively high winter ice edge variability with a low number of in situ ocean observations (see Figure S2 in Supporting Information S1).

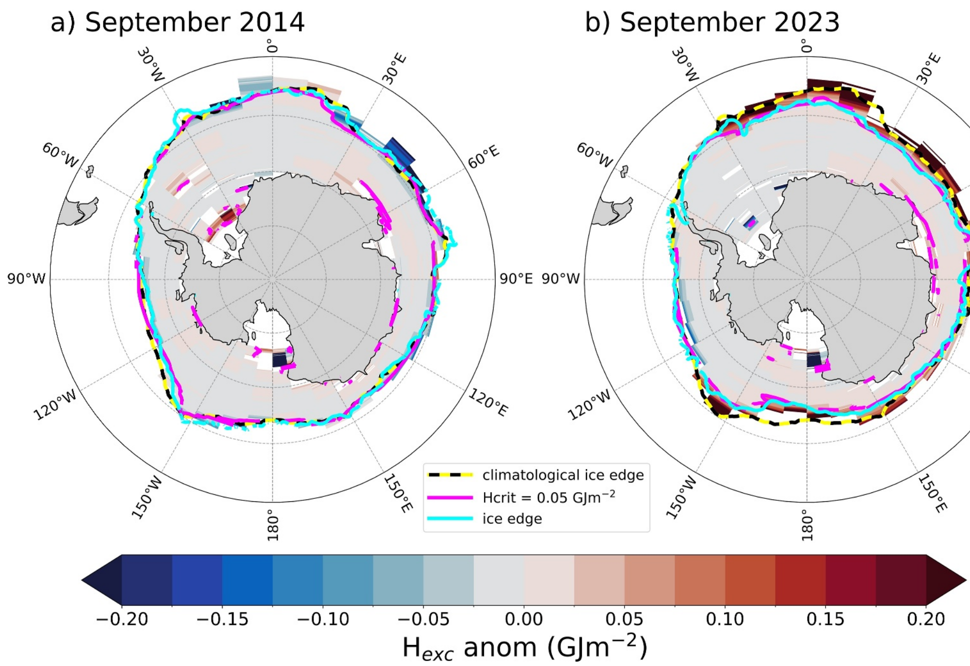

Figure 8. September sea ice and H_{exc} anomalies in (a) 2014 and (b) 2023 from the ORAS5 reanalysis and the NSIDC sea ice observations. Shading shows the H_{exc} anomaly compared to the 2006–2023 mean, the magenta line shows the $H_{\text{exc}} = 0.05$ GJm^{-1} isoline. The black-yellow dashed line shows the climatological sea ice edge and the cyan line shows the ice edge for that year.

In the previous section we posited that H_{exc} could decompose the thermal limits on winter sea ice into contributions from summer warming, winter surface cooling, and subsurface heating over winter (Figure 6). We explore this further by estimating the September H_{exc_prec} for each year using a) H_{exc_prec} that is, February H_{exc} and the surface cooling for that year (red markers/line in Figure 7), and b) H_{exc_pred} (predicted H_{exc}) that is, February H_{exc} and the climatological surface cooling (cyan lines/markers). H_{exc_pred} is a measure of the predictive skill of summer conditions since it does not require knowledge of the true atmosphere state over any winter, and thus provides a physical framework for studies of winter sea ice predictability (e.g., Holland et al., 2013; Libera et al., 2022; Marchi et al., 2018). (Note that whilst this analysis allows an exploration of whether summer H_{exc_pred} has any predictive skill, the primary aim is to extend the decomposition in Section 4.1 to reveal how interannual variability is affected by preconditioning, surface flux and ocean heat.)

For the model H_{exc_prec} calculated using interannually-vary surface fluxes (red line/markers) retains some skill, and the interannual correlations are still statistically significant (Figure 7b). The skill is reduced compared to using actual September ocean conditions, indicating that ocean heat fluxes into the Winter Water layer are an important aspect of the ice edge interannual variability. We note that there is some spatial dependence to this result—some longitudes have lower correlations than others—possibly related to local differences in underlying hydrography (noting that a low correlation here indicates an important contribution from wintertime ocean processes).

The cyan lines/markers show that H_{exc_pred} is much less useful as a predictor of winter sea ice when only the summer ocean conditions are known. The broad spatial structure is still representative (i.e., the blue markers are close to the 1-to-1 line in Figure 7a) but the interannual correlations are no longer statistically significant in either the model or reanalysis. This suggests that summer ocean conditions have little predictive skill for winter sea ice in general, and is consistent with Libera et al. (2022), although studies suggest it may have played a role in recent years (Himmich et al., 2024). As discussed in regard to Figure 6b, H_{exc_prec} systematically underestimates the ice edge latitude (i.e., the cyan and red markers in Figure 7c are above the 1-to-1 line), which we hypothesize is due the representation of the vertical salinity gradient (either biased in the reanalysis, or missing winter processes in the model).

There are several possible reasons why the model has a higher correlation than the reanalysis. The model may well under-represent the effect of parametrized mesoscale features (e.g., ocean mixing), which would inflate the impact of the bulk H_{exc} metric. On the other hand, the observed estimate is a short record that is based on a sparse observation network, leading to uncertainties for some years in H_{exc} (Figure S2 in Supporting Information S1). It should also be noted that in the model, the sea ice and ocean are constrained to be thermodynamically consistent, whereas the observed analysis compares satellite sea ice retrievals with a model assimilating independent in situ ocean profiles.

To demonstrate the benefits of the SaFT metric over the traditional MLD, we also estimate the excess heat preventing sea ice formation by integrating the heat content above T_f to the February MLD (orange markers in Figures 7a and 7c), rather than the shallowest SaFT = 0 isoline per Figure 2. As expected from Figure 2, this consistently overestimates the winter ice edge latitude (i.e., the orange dots lie below the 1-to-1 line), since the MLD does not completely envelop the layer of water that must be cooled as before sea ice formation. It also shows that the MLD-based estimate has very little relationship with the spatially and temporally varying ice edge, and performs significantly worse than either H_{exc_prec} estimate. This result shows that estimating the ocean's thermal limit on sea ice production is not trivial (if it were, then the MLD would produce similar results to H_{exc_prec}) and is further evidence that SaFT is a preferable diagnostic tool than MLD for investigating ocean-sea ice interactions.

This work is partially motivated by recent winters with extreme low sea ice cover. Figure 7 demonstrates that our framework captures interannual variability in the sea ice edge, but we also consider here whether it captures such extreme changes. Figure 8 compares the September H_{exc} and ice edge conditions for 2014 (the largest winter extent on record) and 2023 (the lowest winter extent on record). The differences between the two years are clear, and in particular the 2023 low sea ice extent in the Weddell and Indian Ocean sectors correspond to significant warm H_{exc} anomalies. For both extremely high and extremely low ice cover years, the ice edge corresponds well with the $H_{\mathrm{exc}} \sim 0$ limit.

5. Discussion and Conclusions

Su (2017) showed that a sufficiently strong vertical salinity gradient is a necessary condition for sea ice growth. That condition is formalized here through the property of SaFT, which is a function of both the salinity gradient and the deep ocean temperature. Analysis of a model and reanalysis confirms that the existence of a depth with SaFT < 0 is a necessary condition for sea ice to form, and in the Bellingshausen Sea (west of the Antarctic Peninsula) this sets the absolute limit of the ice edge during winter. In most regions, the removal of heat content within that salinity-stratified layer—which is defined here as excess heat above freezing (H_{exc})—is a further limit on sea ice formation. Such regions (notably the Macquarie Ridge at 150°W, and the Weddell/King Haakon VII Sea at 0–30°E) are identified in Figure 3 as locations with a clear SaFT layer that retains some heat above freezing temperature at the end of winter. This constraint that H_{exc} places on sea ice is much clearer in a numerical model than in reanalysis, but this seems to be at least partially due to the limits of the observing network, and in particular our ability to characterize winter salinity profiles.

The polar Southern Ocean is a strongly coupled ocean-sea ice-atmosphere system. We have shown that halo-stratification is a pre-requisite for sea ice formation over the deep ocean, but it is important to note that this halo-stratification only occurs because of the net surface freshening from sea ice (Pellichero et al., 2018). The relatively low winter ice edge variability suggests that historically this coupled system was somewhat in equilibrium, but recent consecutive winters with extreme low extent (2023, 2024 and 2025) have made the topic of what constrains the maximum ice cover much more pressing. Our results demonstrate that the SaFT metric provides a framework to explore these events, since it can disentangle the thermal and haline effects on upper ocean stability. It can also be used to decompose thermodynamic drivers of winter sea ice cover into contributions from summer preconditioning, winter surface cooling, and internal ocean heat sources over winter. Our analysis shows that all three contribute to winter sea ice extent variability, but which of those has driven recent extremes is yet to be established.

Our analysis clearly demonstrates that the SaFT metric describes the evolution of the polar surface ocean, but a legitimate question is whether it provides valuable information that is not available from already-accepted definitions of the mixed layer, for example, the widely used metric of potential density 0.03 kgm^{-3} greater than the surface (de Boyer Montégut et al., 2004; Levitus, 1982). Firstly, it is essential to note that the purpose of SaFT is to isolate the thermal barrier to sea ice growth, rather than to address the more general feature of a turbulent mixed layer. In practice the two are related, in that once the upper ocean has cooled enough to allow a surface temperature of T_f, the excess heat would be zero whether integrated to the SaFT layer or to the MLD (as indicated in Figures 5a and 5d). However, the advantage of our framework over MLD is that it can decompose the thermodynamic limits of winter sea ice cover into thermal and haline components (Figure 2d), and into the contributions from summer preconditioning, winter surface cooling, and internal ocean heat sources (Figures 6 and 7). Such a decomposition is nominally possible using MLD, but the true layer of summer surface water that must be cooled to allow surface freezing is somewhat deeper than the MLD (Figure 2), leading to a low bias in H_{exc}. This results in a quantitively incorrect diagnosis that has little relationship to the interannually varying winter sea ice edge (Figure 7).

A further advantage of the SaFT approach is that we can rigorously define not just a single mixed layer, but the multiple shallow layers that form in the polar ocean at different months. Specifically, the summer polar Southern Ocean has a remnant of the previous winter's cold surface water (remnant Winter Water; rWW) that is capped by a fresh warm surface layer formed by sea ice melt. Our SaFT method isolates the boundary between these two. Furthermore, in winter the boundary between the Winter Water and the warmer CDW is very important, since it marks where entrainment of CDW to the surface occurs (Martinson & Iannuzzi, 1998). The SaFT method identifies this boundary. Whilst multiple definitions of Winter Water exist that can be applied to the polar environment (reviewed by Spira et al., 2024), they are empirical whereas the SaFT criterion has a clear physical basis based on the ability to maintain a freezing temperature at the surface. Finally, many density-based criteria are based on an empirical coincidence with the seasonal thermocline, which may have less relevance in the polar ocean, especially in winter when salinity-driven buoyancy forcing may dominate over wind-driven mixing (Bennetts et al., 2024; Koenig et al., 2020).

It should be noted that both SaFT and H_{exc} are simple thermodynamic estimates, and cannot account for mesoscale features in the ocean, or sea ice motion that can transport sea ice north of the ice H_{exc} limit (Figure 4). The analysis in this work shows that this bulk approach still has validity at the relatively coarse spatial scales considered here (more than 10° longitude resolution) and is certainly an appropriate tool for analyzing sector or circumpolar SIA.

A more serious weakness is the limit imposed by the sparse observation network. The under-ice Argo program has significantly increased coverage, especially at latitudes typical of the winter ice edge; the Antarctic continental shelf is much more poorly observed. However, there are still significant observation gaps, especially in East Antarctica. Given the global importance of the Southern Ocean for anthropogenic heat and carbon uptake (e.g., Frolicher et al., 2015; Williams et al., 2023), and the possibility that recent sea ice extremes represent a significant change (Hobbs et al., 2024), this research highlights the need for sustained circumpolar monitoring of the polar Southern Ocean.

Conflict of Interest

The authors declare no conflicts of interest relevant to this study.

Data Availability Statement

ORAS5 data were obtained from the Copernicus Climate data store (Copernicus Climate Change Service, 2021), and are available under a CC-BY license. The Climate Data Record of Passive Microwave Sea ice Concentration data were obtained from Meier et al. (2021). The ACCESS-OM2-025 data used in this study are publicly available from Holmes et al. (2025). All code used in this analysis is available from a public repository (Hobbs, 2025).

Acknowledgments
This project received Grant funding from the Australian Government as part of the Antarctic Science Collaboration Initiative program, and the Australian Research Council (ARC) Discovery Project DP 230102994, ARC Discovery Early Career Researcher Award (DE21010004) and ARC Linkage Project LP200100406. This work was supported by computational resources provided by the Australian Government through the National Computational Infrastructure (NCI) under the National Computational Merit Allocation Scheme and ANU Merit Allocation Scheme. We thank the Consortium for Ocean–Sea Ice Modeling in Australia (COSIMA; cosima.org.au) for making the ACCESS-OM2 models, outputs and analysis tools available through the NCI. Open access publishing facilitated by University of Tasmania, as part of the Wiley - University of Tasmania agreement via the Council of Australian University Librarians.

References

Abernathey, R. P., Cerovecki, I., Holland, P. R., Newsom, E., Mazlo, M., & Talley, L. D. (2016). Water-mass transformation by sea ice in the upper branch of the Southern Ocean overturning. *Nature Geoscience*, *9*(8), 596–601. https://doi.org/10.1038/Ngeo2749

Bennetts, L. G., Shakespeare, C. J., Vreugdenhil, C. A., Foppert, A., Gayen, B., Meyer, A., et al. (2024). Closing the loops on Southern Ocean dynamics: From the circumpolar current to ice shelves and from bottom mixing to surface waves. *Reviews of Geophysics*, *62*(3), e2022RG000781. https://doi.org/10.1029/2022RG000781

Copernicus Climate Change Service. (2021). ORAS5 global ocean reanalysis monthly data from 1958 to present. https://doi.org/10.24381/CDS.67E8EEB7

de Boyer Montégut, C., Madec, G., Fischer, A. S., Lazar, A., & Iudicone, D. (2004). Mixed layer depth over the global ocean: An examination of profile data and a profile-based climatology. *Journal of Geophysical Research*, *109*(C12). https://doi.org/10.1029/2004JC002378

Eayrs, C., Li, X., Raphael, M. N., & Holland, D. M. (2021). Rapid decline in Antarctic sea ice in recent years hints at future change. *Nature Geoscience*, *14*(7), 460–464. https://doi.org/10.1038/s41561-021-00768-3

Frolicher, T. L., Sarmiento, J. L., Paynter, D. J., Dunne, J. P., Krasting, J. P., & Winton, M. (2015). Dominance of the Southern Ocean in anthropogenic carbon and heat uptake in CMIP5 models. *Journal of Climate*, *28*(2), 862–886. https://doi.org/10.1175/Jcli-D-14-00117.1

Gilbert, E., & Holmes, C. (2024). 2023's Antarctic sea ice extent is the lowest on record. *Weather*, *79*(2), 46–51. https://doi.org/10.1002/wea.4518

Hersbach, H., Bell, B., Berrisford, P., Hirahara, S., Horányi, A., Muñoz-Sabater, J., et al. (2020). The ERA5 global reanalysis. *Quarterly Journal of the Royal Meteorological Society*, *146*(730), 1999–2049. https://doi.org/10.1002/qj.3803

Himmich, K., Vancoppenolle, M., Madec, G., Sallée, J.-B., Holland, P. R., & Lebrun, M. (2023). Drivers of Antarctic sea ice advance. *Nature Communications*, *14*(1), 6219. https://doi.org/10.1038/s41467-023-41962-8

Himmich, K., Vancoppenolle, M., Stammerjohn, S., Bocquet, M., Madec, G., Sallée, J.-B., & Fleury, S. (2024). Thermodynamics drive Post-2016 changes in the Antarctic Sea ice seasonal cycle. *Journal of Geophysical Research: Oceans*, *129*(8), e2024JC021112. https://doi.org/10.1029/2024JC021112

Hobbs, W. (2025). willrhobbs/SaFT_paper: Ocean constraints on winter Antarctic sea ice extent (version v1.0). *Zenodo*. https://doi.org/10.5281/ZENODO.17585394

Hobbs, W., Massom, R., Stammerjohn, S., Reid, P., Williams, G. D., & Meier, W. N. (2016). A review of recent changes in Southern Ocean Sea ice, their drivers and forcings. *Global and Planetary Change*, *143*, 228–250. https://doi.org/10.1016/j.gloplacha.2016.06.008

Hobbs, W., Spence, P., Meyer, A., Schroeter, S., Fraser, A., Reid, P., et al. (2024). Observational evidence for a regime shift in summer Antarctic sea ice. *Journal of Climate*, *37*(7), 2263–2275. https://doi.org/10.1175/JCLI-D-23-0479.1

Holland, M. M., Blanchard-Wrigglesworth, E., Kay, J., & Vavrus, S. (2013). Initial-value predictability of Antarctic sea ice in the Community climate system model 3. *Geophysical Research Letters*, *40*(10), 2121–2124. https://doi.org/10.1002/grl.50410

Holmes, R., Hobbs, W., & Kiss, A. E. (2025). ACCESS-OM2-025 simulation output for Hobbs et al. (2025) "Ocean constraints on winter Antarctic sea ice extent". *Zenodo*. https://doi.org/10.5281/ZENODO.16899538

Kiss, A. E., Hogg, A. M., Hannah, N., Boeira Dias, F., Brassington, G. B., Chamberlain, M. A., et al. (2020). ACCESS-OM2 v1.0: A global ocean–sea ice model at three resolutions. *Geoscientific Model Development*, *13*(2), 401–442. https://doi.org/10.5194/gmd-13-401-2020

Koenig, Z., Fer, I., Kolås, E., Fossum, T. O., Norgren, P., & Ludvigsen, M. (2020). Observations of turbulence at a near-surface temperature front in the Arctic Ocean. *Journal of Geophysical Research: Oceans*, *125*(4), e2019JC015526. https://doi.org/10.1029/2019JC015526

Levitus, S. (1982). *Climatological atlas of the world ocean* (Vol. 13). US Department of Commerce, National Oceanic and Atmospheric Administration.

Libera, S., Hobbs, W., Klocker, A., Meyer, A., & Matear, R. (2022). Ocean-Sea ice processes and their role in multi-month predictability of Antarctic Sea ice. *Geophysical Research Letters*, *49*(8), e2021GL097047. https://doi.org/10.1029/2021gl097047

Liu, J., Zhu, Z., & Chen, D. (2023). Lowest antarctic Sea ice record broken for the second year in a row. *Ocean-Land-Atmosphere Research*, *2*, 7. https://doi.org/10.34133/olar.0007

Marchi, S., Fichefet, T., Goosse, H., Zunz, V., Tietsche, S., Day, J. J., & Hawkins, E. (2018). Reemergence of Antarctic sea ice predictability and its link to deep ocean mixing in global climate models. *Climate Dynamics*, *52*(5–6), 2775–2797. https://doi.org/10.1007/s00382-018-4292-2

Martinson, D. G. (1990). Evolution of the southern-ocean Winter mixed layer and Sea ice - Open ocean deep-water formation and ventilation. *Journal of Geophysical Research*, *95*(C7), 11641–11654. https://doi.org/10.1029/Jc095ic07p11641

Martinson, D. G., & Iannuzzi, R. A. (1998). Antarctic ocean-ice interaction: Implications from ocean bulk property distributions in the weddell gyre. In *Antarctic sea ice: Physical processes, interactions and variability* (pp. 243–271).

Meier, W. N., Fetterer, F., Windnagel, A. K., & Stewart, J. S. (2021). NOAA/NSIDC climate data record of passive microwave sea ice concentration, version 4. Retrieved from: https://nsidc.org/data/g02202/versions/4

Nihashi, S., & Ohshima, K. I. (2015). Circumpolar mapping of Antarctic coastal polynyas and Landfast Sea Ice: Relationship and variability. *Journal of Climate*, *28*(9), 3650–3670. https://doi.org/10.1175/JCLI-D-14-00369.1

Pellichero, V., Sallée, J.-B., Chapman, C. C., & Downes, S. M. (2018). The southern ocean meridional overturning in the sea-ice sector is driven by freshwater fluxes. *Nature Communications*, *9*(1), 1789. https://doi.org/10.1038/s41467-018-04101-2

Pellichero, V., Sallee, J. B., Schmidtko, S., Roquet, F., & Charrassin, J. B. (2017). The ocean mixed layer under Southern Ocean sea-ice: Seasonal cycle and forcing. *Journal of Geophysical Research-Oceans*, *122*(2), 1608–1633. https://doi.org/10.1002/2016jc011970

Purich, A., & Doddridge, E. W. (2023). Record low Antarctic sea ice coverage indicates a new sea ice state. *Communications Earth & Environment*, *4*(1), 314. https://doi.org/10.1038/s43247-023-00961-9

Raphael, M. N., & Handcock, M. S. (2022). A new record minimum for Antarctic sea ice. *Nature Reviews Earth & Environment*, *3*(4), 215–216. https://doi.org/10.1038/s43017-022-00281-0

Roquet, F., Ferreira, D., Caneill, R., Schlesinger, D., & Madec, G. (2022). Unique thermal expansion properties of water key to the formation of sea ice on Earth. *Science Advances*, *8*(46), eabq0793. https://doi.org/10.1126/sciadv.abq0793

SOOS. (2023). SOOS Statement 2023. In *Paper presented at the inaugral SOOS symposium: Southern Ocean in a changing world*.

Spira, T., Swart, S., Giddy, I., & du Plessis, M. (2024). The observed spatiotemporal variability of antarctic Winter water. *Journal of Geophysical Research: Oceans*, *129*(10), e2024JC021017. https://doi.org/10.1029/2024JC021017

Su, Z. (2017). Preconditioning of Antarctic maximum sea ice extent by upper ocean stratification on a seasonal timescale. *Geophysical Research Letters*, *44*(12), 6307–6315. https://doi.org/10.1002/2017gl073236

Turner, J., Phillips, T., Marshall, G. J., Hosking, J. S., Pope, J. O., Bracegirdle, T. J., & Deb, P. (2017). Unprecedented springtime retreat of Antarctic sea ice in 2016. *Geophysical Research Letters*, *44*(13), 6868–6875. https://doi.org/10.1002/2017gl073656

Wang, H., Klekociuk, A. R., French, W. J. R., Alexander, S. P., & Warner, T. A. (2020). Measurements of Cloud Radiative Effect across the Southern Ocean (43°S–79°S, 63°E–158°W). *Atmosphere*, *11*(9), 949. https://doi.org/10.3390/atmos11090949

Wang, J., Massonnet, F., Goosse, H., Luo, H., Barthélemy, A., & Yang, Q. (2024). Synergistic atmosphere-ocean-ice influences have driven the 2023 all-time Antarctic sea-ice record low. *Communications Earth & Environment*, *5*(1), 415. https://doi.org/10.1038/s43247-024-01523-3

Williams, R. G., Ceppi, P., Roussenov, V., Katavouta, A., & Meijers, A. J. S. (2023). The role of the Southern Ocean in the global climate response to carbon emissions. *Philosophical Transactions of the Royal Society A: Mathematical, Physical and Engineering Sciences*, *381*(2249), 20220062. https://doi.org/10.1098/rsta.2022.0062

Wilson, E. A., Riser, S. C., Campbell, E. C., & Wong, A. P. S. (2019). Winter upper-ocean stability and ice–ocean feedbacks in the Sea ice–covered Southern Ocean. *Journal of Physical Oceanography*, *49*(4), 1099–1117. https://doi.org/10.1175/JPO-D-18-0184.1

Zuo, H., Balmaseda, M. A., Tietsche, S., Mogensen, K., & Mayer, M. (2019). The ECMWF operational ensemble reanalysis–analysis system for ocean and sea ice: A description of the system and assessment. *Ocean Science*, *15*(3), 779–808. https://doi.org/10.5194/os-15-779-2019